Kohn anomaly of optical zone boundary phonons in uniaxial strained graphene: Role of the Dirac cone electronic dispersion

Sonia Haddad* and Lassaad Mandhour
Laboratoire de Physique de la Matière Condensée, Département de Physique, Faculté des Sciences de Tunis, Université Tunis El Manar, Campus Universitaire 1060 Tunis, Tunisia

(Received 28 March 2018; revised manuscript received 26 July 2018; published 10 September 2018)

One of the unique properties of graphene is its extremely high mechanical strength. Several studies have shown that the mechanical failure of a graphene sheet under a tensile strain is due to the enhancement of the Kohn anomaly of the zone boundary transverse optical phonon modes. In this work, we derive an analytical expression of the Kohn anomaly parameter $\alpha_{\vec{K}}$ of these phonons in graphene deformed by a uniaxial strain along the armchair direction. We show that the tilt of Dirac cones, induced by the strain, contributes to the enhancement of the Kohn anomaly under a tensile deformation and gives rise to a dominant contribution of the so-called *outer* intervalley-mediated phonon processes. Moreover, the Kohn anomaly is found to be anisotropic with respect to the phonon wave vectors around the K point. This anisotropy may be at the origin of the light polarization dependence of the Raman 2D band of the strained graphene. Our results not only uncover the role of the Kohn anomaly in the anisotropic mechanical failure of the graphene sheet under strains applied along the armchair and zigzag directions, but they also shed light on the doping-induced strengthening of strained graphene.

DOI: 10.1103/PhysRevB.98.115420

I. INTRODUCTION

Despite the unique features of graphene, several drawbacks have to be overcome to integrate this material in optoelectronic devices. In particular, the lack of a band gap is a problem standing in the way of using graphene in electronics [1,2]. Moreover, it has been proven that it is not possible to obtain high-temperature intrinsic superconductivity in this material regarding the weak electron-phonon coupling responsible for the superconducting state [3].

In the past few years, strain engineering has emerged as a powerful tool to control the optical and electronic properties of two-dimensional (2D) materials [4–8]. Strained graphene has recently become a hot topic of interest since it is expected to pave the way for new applications for flexible electronic devices in which the graphene sheet is manipulated like a piece of origami paper [5,9].

Deformed graphene under strain may also offer new physical insights, e.g., the generation of exotic electronic states under a giant pseudomagnetic field [10] and relatively high-temperature superconductivity at $T_c \sim 30$ K [11,12]. Although the vibrational spectrum of graphene is significantly changed under strain, no band gap has been induced in the electronic dispersion up to the critical strain amplitude $\epsilon \sim 20\%$ [13] before sample cracking [14–16]. However, it is found that under uniaxial strain, the Dirac points shift from the high-symmetry points K and K' located at the corner of the hexagonal Brillouin zone [1,14,17].

The signature of the strain on the electronic and vibrational properties of graphene could be probed by Raman spectroscopy, which is found to be sensitive to the strain [18–31]. In particular, the G peak, originating from the doubly degenerate E_{2g} zone center phonons, splits into two peaks whose intensities are strongly dependent on the incident light polarization [22]. This dependence is found to be the fingerprint of the strain modified electronic dispersion, which affects the Raman G band through the electron-phonon interaction [32].

Due to its higher strain-induced frequency shift, the 2D Raman peak is commonly used to determine the strength and the direction of the applied strain [19,21,24,27,30,33,34]. This peak is due to the doubly resonant intervalley process involving transverse optical boundary phonons with wave vector $\vec{K}$ [18]. The characteristic features of the 2D band under strain are found to be substantially dependent on both the electronic structure and the dispersion of the in-plane transverse optical phonon (iTO) mode at the K point [27–30]. This dispersion is marked by a remarkable Kohn anomaly (KA) revealed by a pronounced kink, which reflects strong electron-phonon coupling (EPC) [35–40].

The KA occurs in metals due to the electron screening of the ionic potential [41]. This anomaly appears in the phonon branch as a sudden dip at a phonon wave vector $\vec{q}$ connecting two electronic states $\vec{k}$ and $\vec{k}'$ on the Fermi surface satisfying $\vec{k}' = \vec{k} + \vec{q}$.

In graphene, the KA takes place at Γ ($\vec{q} = \vec{0}$) and at the K point ($\vec{q} = \vec{K}$) since the Fermi surface was reduced to the two points K and K' [42]. KA in nondeformed graphene has been studied under close scrutiny [42–46] since it measures electron-phonon coupling, which is a key parameter to understand several properties of graphene, such as the electronic transport, the stability of the superconducting state, and the Raman spectra.

However, a few studies can be found in the literature on the behavior of the KA in strained graphene. The role of the

*sonia.haddad@fst.utm.tn

KA has been shown to be crucial for the mechanical failure process of pure graphene [47,48]. Si *et al.* [48] reported, based on first-principles calculations, that the strain-induced enhancement of the KA in graphene could be counterbalanced by doping. Recently, Cifuentes-Quintal *et al.* [49] showed that, besides the pronounced KA of the transverse optical phonon modes, a new KA emerges under a uniaxial strain in the longitudinal acoustic phonon branch around the K point.

The outcomes of the studies, dealing with the behavior of the KA in strained graphene, raised several open questions. In particular, it is not understood why the doping-induced weakening of the KA is much more pronounced in the strained graphene than in the unstrained lattice. On the other hand, the origin of the anisotropic failure mechanism of a graphene sheet under zigzag and armchair tensile deformations is not completely unveiled [50–67]. Moreover, the behavior of the 2D Raman band under strain is still under debate. In addition to the vigorous debate on the type of optical phonons responsible for these bands, the origin of their light polarization dependence is still not fully understood [30,31].

Based on an analytical analysis of the KA mechanism in strained graphene, we try, in this paper, to provide some answers to the above-mentioned puzzling points. We consider a honeycomb lattice under uniaxial strain applied along the armchair edges (y axis). We neglect, hereafter, the strain component ϵ_{xx} along the x axis perpendicular to the strain direction regarding the small value of the Poisson ratio of graphene ($\nu = 0.165$). This ratio relates the strain components as $\epsilon_{xx} = -\nu\epsilon_{yy}$ [14,32]. This approximation, which is useful to derive an analytical expression for the KA slope, is justified regarding the small values of the strain amplitude and the Poisson ratio of graphene.

Moreover, we do not consider the strain effect on the phonon band in order to highlight the signature of the electronic dispersion. Such an approximation was also used in Ref. [30] to study the strain-induced splitting of the 2D Raman band.

The main results of this work can be summarized in the following points: (i) The strain-modified electronic dispersion affects substantially the KA. In particular, the tilt of Dirac cones is found to enhance the KA under a tensile deformation and to further the so-called *outer* phonon-mediated intervalley electronic transitions. (ii) The KA shows an anisotropic behavior as a function of the phonon wave vector around the zone boundary K point. This anisotropy contributes to the light polarization dependence of the 2D Raman peak in strained graphene. (iii) The weakening of the KA with electronic doping is found to be more pronounced in strained graphene than in an unstrained lattice. (iv) The KA behavior gives rise to a large critical tensile deformation along the zigzag (ZZ) direction compared to the armchair axis, in agreement with the numerical calculations [50,52,54,55,60,61].

The paper is organized as follows: In Sec. II, we derive the EPC expression for the graphene in-plane TO phonon mode. The behavior of the KA of these phonons is discussed in Sec. III. Section IV is devoted to concluding remarks.

II. ELECTRON-PHONON COUPLING: EFFECTIVE-MASS APPROACH

A. Transverse optical phonon mode: KA slope

We focus on the highest optical phonon branch at the K point corresponding to the A_1' mode showing a KA at a frequency $\omega_K = 161$ meV [42]. In graphene, the Fermi surface reduces to the points K and K', and the density of states N_F at the Fermi energy is zero. As a consequence, the usual EPC coupling constant $\lambda_{\vec{q}}$, depending on $1/N_F$, is not well defined [42]. Therefore, the EPC in graphene is characterized instead by the ratio $2\langle g_{\vec{q}}^2\rangle_F/\hbar\omega_{\vec{q}}$, where $2\langle g_{\vec{q}}^2\rangle_F$ is the average over the Fermi surface of $|g_{\vec{k}+\vec{q},\lambda;\vec{k}\lambda'}|^2$, and $g_{\vec{k}+\vec{q},\lambda;\vec{k}\lambda'}$ is the coupling matrix element of the phonon with a wave vector $\vec{q}$ and electrons in the state $\vec{k}$ within the band λ, which scatter to the λ' band at the state $\vec{k}' = \vec{k} + \vec{q}$ [42].

In nondeformed graphene, the largest value of EPC is found for the A_1' mode for which $2\langle g_K^2\rangle_F/\hbar\omega_{\vec{K}} = 1.23$ eV [42]. This mode exhibits a KA described by a nonzero slope $\alpha_{\vec{K}}$ of the phonon dispersion, which can be written around the K point as $\omega_{\vec{K}+\vec{q}} = \alpha_{\vec{K}}|\vec{q}| + \hbar\omega_{\vec{K}} + O(q^2)$ [42]. $\alpha_{\vec{K}}$ is related to the EPC by [42]

$$\alpha_{\vec{K}} = \hbar \lim_{\vec{q}\to\vec{0}} \frac{\omega_{\vec{K}+\vec{q}} - \omega_{\vec{K}}}{q} = \hbar \lim_{\vec{q}\to\vec{0}} \frac{\tilde{D}_{\vec{K}+\vec{q}} - \tilde{D}_{\vec{K}}}{2\omega_{\vec{K}} M q}, \quad (1)$$

where $q = |\vec{q}|$, M is the carbon atomic mass, and $\tilde{D}_{\vec{q}}$ is the nonanalytic component of the dynamical matrix [42] given by

$$\tilde{D}_{\vec{q}} = \frac{8M\omega_{\vec{K}}}{\hbar}\frac{S}{(2\pi^2)}\int d\vec{k}\frac{|g_{2\vec{K}+\vec{k}+\vec{q},\pi^*;\vec{K}+\vec{k},\pi}|^2}{\varepsilon_{\vec{K}+\vec{k},\pi} - \varepsilon_{2\vec{K}+\vec{k}+\vec{q},\pi^*}}, \quad (2)$$

where the transition of an electron from the occupied band (π) of the K valley to the empty band (π^*) of the valley K' ($\vec{K}' = 2\vec{K}$) is considered. S is the crystal surface.

In nondeformed graphene, the matrix element is of the form

$$|g_{2\vec{K}+\vec{k}+\vec{q},\pi^*;\vec{K}+\vec{k},\pi}|^2 = \langle g_K^2\rangle_F(1+\cos\theta), \quad (3)$$

with θ being the angle between $\vec{k}$ and $\vec{k}+\vec{q}$ [42].

Considering the linear electronic dispersion around the Dirac points, $\alpha_{\vec{K}}$ becomes [42]

$$\alpha_{\vec{K}} = \frac{8\langle g_K^2\rangle_F}{\hbar v_F}\frac{S}{(2\pi^2)}\lim_{\vec{q}\to\vec{0}}\int_{k<k_m} d\vec{k}\left[\frac{1}{k} - \frac{1+\cos\theta}{k+|\vec{k}+\vec{q}|}\right], \quad (4)$$

where v_F is the Fermi velocity and k_m is a cutoff corresponding to the limit of the linear dispersion of the electronic band. The numerical integration of the above expression gives $\alpha_{\vec{K}} \sim 253$ cm^{-1} Å [42,44].

In the following, we derive the expression of the KA slope $\alpha_{\vec{K}}$ in strained graphene. We first start by determining the EPC matrix element $g_{2\vec{K}+\vec{k}+\vec{q},\pi^*;\vec{K}+\vec{k},\pi}$.

B. EPC in strained graphene

1. Electronic Hamiltonian

We assume that the uniaxial strain is along the armchair (AC) direction, denoted by the y axis, which results in a quinoid lattice [68] as shown in Fig. 1.

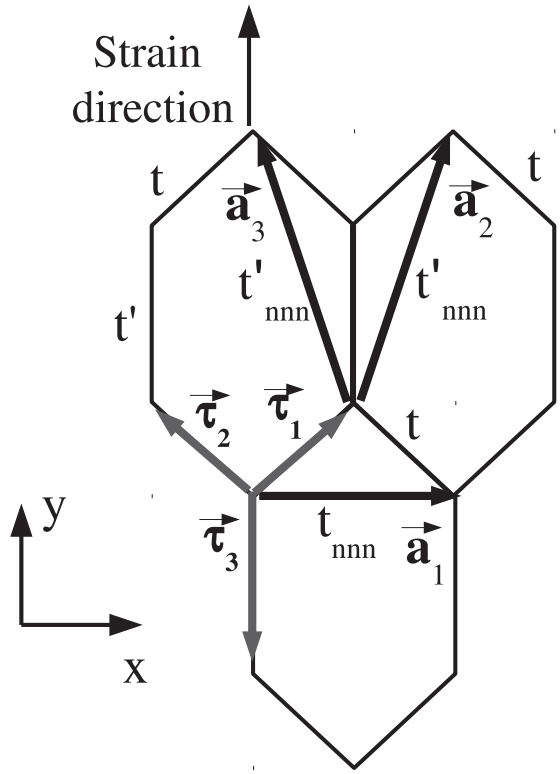

FIG. 1. Deformed honeycomb lattice along the armchair y axis. $(\vec{a}_1, \vec{a}_2)$ is the lattice basis. The hopping parameters to the first (second) neighbors t and t' (t_{nnn} and t'_{nnn}) are different due to the deformation. Vectors connecting first (second) neighboring atoms are denoted $\vec{\tau}_l$ ($\vec{a}_l$).

The distance between nearest-neighbor atoms along the strain axis changes from a to $a' = a + \delta a = a(1+\epsilon)$, where $\epsilon = \frac{\delta a}{a}$ is the lattice deformation or the strain amplitude. For a compressive (tensile) deformation, ϵ is negative (positive). The lattice basis is given by $(\vec{a}_1, \vec{a}_2)$, where

$$\vec{a}_1 = \sqrt{3}a\vec{e}_x, \quad \vec{a}_2 = \frac{\sqrt{3}}{2}a\vec{e}_x + a\left(\frac{3}{2}+\epsilon\right)\vec{e}_y. \tag{5}$$

The vectors joining the first-neighbor atoms are

$$\vec{\tau}_1 = \frac{a}{2}(\sqrt{3}\vec{e}_x + \vec{e}_y), \quad \vec{\tau}_2 = \frac{a}{2}(-\sqrt{3}\vec{e}_x + \vec{e}_y),$$
$$\vec{\tau}_3 = -a(1+\epsilon)\vec{e}_y. \tag{6}$$

The hopping integral along the $\vec{\tau}_3$ direction is modified by the strain from t to $t' = t + \frac{\partial t}{\partial a}\delta a$. The hopping terms to the second neighboring atoms t_{nnn} change also compared to their values in undeformed graphene as

$$t'_{nnn} = t_{nnn} + \frac{\partial t_{nnn}}{\partial a}\delta a. \tag{7}$$

Assuming the Harrison law [69], $\frac{\partial t}{\partial a} = -\frac{2t}{a}$, then t' reduces to

$$t' = t(1-2\epsilon). \tag{8}$$

It is worth noting that, beyond the linear elastic regime, the Harrison law is not accurate enough to deal with the strain-induced changes of the hopping integrals [70]. For a more accurate approach, it has been proposed to consider the hopping parameters deduced from density functional theory (DFT) calculations [71].

The quinoid lattice could be described by the so-called minimal form of the generalized 2D Weyl Hamiltonian [69,72] given by

$$H_\xi(\vec{k}) = \xi(\vec{w}_0 \cdot \vec{k}\sigma^0 + w_x k_x \sigma^x) + w_y k_y \sigma^y, \tag{9}$$

where $\sigma^0 = \mathbb{1}$, σ^x and σ^y are the 2×2 Pauli matrices, ξ is the valley index, w_x and w_y characterize the anisotropy of the Dirac cones, whereas $\vec{w}_0$ is the tilt term. These parameters could be expressed, for a small deformation amplitude ($|\epsilon| \ll 1$), as [69]

$$w_x = \frac{3}{2}at\left(1+\frac{2}{3}\epsilon\right), \quad w_y = \frac{3}{2}at\left(1-\frac{4}{3}\epsilon\right),$$
$$\vec{w}_0 = (w_{0x} = 0.6\,\epsilon\, w_x, w_{0y} = 0). \tag{10}$$

The Hamiltonian given by Eq. (9) is derived within a tight-binding approach [68]. It can be obtained using a transformation combining the strain tensor and rotations, as was done in Refs. [73,74], or a gauge field approach [75–77].

The eigenenergies of the Weyl Hamiltonian, given by Eq. (9), are [69]

$$\varepsilon_\lambda(\vec{k}) = \xi\,\vec{w}_0 \cdot \vec{k} + \lambda\sqrt{w_x^2 k_x^2 + w_y^2 k_y^2}, \tag{11}$$

where λ is the band index.

The corresponding eigenfunctions are of the form

$$|\lambda, \vec{k}\rangle_D = \frac{1}{\sqrt{2S'}}e^{i\vec{k}\cdot\vec{r}}\begin{pmatrix}\lambda\\ e^{i\Phi(\vec{k})}\end{pmatrix},$$
$$|\lambda, \vec{k}\rangle_{D'} = \frac{1}{\sqrt{2S'}}e^{i\vec{k}\cdot\vec{r}}\begin{pmatrix}e^{i\Phi(\vec{k})}\\ \lambda\end{pmatrix}, \tag{12}$$

where $\Phi(\vec{k})$ is given by

$$\tan\Phi(\vec{k}) = \frac{w_y k_y}{w_x k_x}. \tag{13}$$

Under the strain, the Dirac cones are no longer at the high-symmetry points K and K' but move according to [69]

$$k_y^D = 0, \quad k_x^D = \xi\frac{2}{\sqrt{3}a}\arccos\left(-\frac{t'}{2t}\right). \tag{14}$$

2. *Electron-phonon coupling*

We consider the effective-mass approach, the so-called $\vec{k}\cdot\vec{p}$ method, to derive the Hamiltonian describing the interaction between the electrons and the zone boundary transverse optical phonons in uniaxial strained graphene. This Hamiltonian could be obtained considering the effect of the lattice displacements on the hopping integrals in the undeformed electronic Hamiltonian. This approach was used by Ando [78] in the case of undeformed graphene to obtain the EPC in the case of the highest frequency zone boundary optical phonon mode. The authors applied the $\vec{k}\cdot\vec{p}$ method for the electronic states around the Dirac valleys. Within this method, the electronic wave function could be written as [79,80]

$$\psi(\vec{r}) = \sum_{\vec{R}_A}\psi_A(\vec{R}_A)\varphi(\vec{r}-\vec{R}_A) + \sum_{\vec{R}_B}\psi_B(\vec{R}_B)\varphi(\vec{r}-\vec{R}_B), \tag{15}$$

where $\varphi(\vec{r}-\vec{R}_A)$ and $\varphi(\vec{r}-\vec{R}_B)$ are the atomic orbitals centered on atoms A and B, respectively. The coefficients $\psi_A(\vec{R}_A)$ and $\psi_B(\vec{R}_B)$ are expressed in terms of slowly varying envelope functions F_A^D, $F_A^{D'}$, F_B^D, and $F_B^{D'}$ [78]:

$$\psi_A(\vec{R}_A) = e^{i\vec{k}^D\cdot\vec{R}_A}F_A^D(\vec{R}_A) + e^{i\vec{k}^{D'}\cdot\vec{R}_A}F_A^{D'}(\vec{R}_A),$$
$$\psi_B(\vec{R}_B) = e^{i\vec{k}^D\cdot\vec{R}_B}F_B^D(\vec{R}_B) - e^{i\vec{k}^{D'}\cdot\vec{R}_B}F_B^{D'}(\vec{R}_B). \quad (16)$$

The Weyl Hamiltonian given by Eq. (9) could be derived within the $\vec{k}\cdot\vec{p}$ method taking into account the hopping terms to the second nearest neighbors [32]. The eigenproblem is written as

$$\varepsilon\psi_A(\vec{R}_A) = -\sum_{l=1}^{3} t^{(l)}\psi_B(\vec{R}_A-\vec{\tau}_l) - \sum_{l=1}^{6} t_{nnn}^{(l)}\psi_A(\vec{R}_A-\vec{a}_l),$$
$$\varepsilon\psi_B(\vec{R}_B) = -\sum_{l=1}^{3} t^{(l)}\psi_A(\vec{R}_B+\vec{\tau}_l) - \sum_{l=1}^{6} t_{nnn}^{(l)}\psi_B(\vec{R}_B-\vec{a}_l), \quad (17)$$

where $\vec{a}_4=-\vec{a}_1$, $\vec{a}_5=-\vec{a}_2$, $\vec{a}_6=-\vec{a}_3$, and $t^{(l)}$ ($t_{nnn}^{(l)}$) are the hopping integrals to the first (second) neighboring atoms along $\vec{\tau}_l$ ($\vec{a}_l$) vectors.

Considering the effect of the lattice vibrations on the hopping integrals generates an extra term in Eq. (17) expressing the correction to these hopping integrals. This term gives rise to the EPC Hamiltonian [32].

For simplicity we consider, as in Refs. [42,78], the effect of lattice displacements on the hopping integral $t^{(l)}$ between first neighboring atoms located at $\vec{R}_A$ and $\vec{R}_A-\vec{\tau}_l$. Due to the lattice vibration, this integral changes to

$$t^{(l)} + \frac{\partial t^{(l)}}{\partial d_l}[|\vec{\tau}_l + \vec{u}_A(\vec{R}_A) - \vec{u}_B(\vec{R}_A-\vec{\tau}_l)| - d_l], \quad (18)$$

where $d_l=|\vec{\tau}_l|$, $d_1=d_2=a$, and $d_3=a(1+\epsilon)$. $\vec{u}_A(\vec{R}_A)$ and $\vec{u}_B(\vec{R}_B=\vec{R}_A-\vec{\tau}_l)$ are the lattice displacements.

For the zone boundary optical phonon modes of a wave vector $\vec{q}$, taken around the Dirac points D and D', these displacements could be written as [78]

$$\vec{u}_A(\vec{R}_A) = e^{i\vec{k}^D\cdot\vec{R}_A}\vec{u}_A^D(\vec{R}_A) + e^{i\vec{k}^{D'}\cdot\vec{R}_A}\vec{u}_A^{D'}(\vec{R}_A),$$
$$\vec{u}_B(\vec{R}_B) = e^{i\vec{k}^D\cdot\vec{R}_B}\vec{u}_B^D(\vec{R}_B) + e^{i\vec{k}^{D'}\cdot\vec{R}_B}\vec{u}_B^{D'}(\vec{R}_B). \quad (19)$$

The coefficients $\vec{u}_A^D(\vec{r})$, $\vec{u}_A^{D'}(\vec{r})$, $\vec{u}_B^D(\vec{r})$, and $\vec{u}_B^{D'}(\vec{r})$ are given by

$$\vec{u}_{A/B}^{D/D'}(\vec{r}) = \sum_{\mu,\vec{q}}\sqrt{\frac{\hbar}{2NM\omega_\mu(\vec{q})}}\vec{e}_{A/B,\mu}^{D/D'}(\vec{q}) \times\left(b_{D,\mu,\vec{q}} + b_{D',\mu,-\vec{q}}^{\dagger}\right)e^{i\vec{q}\cdot\vec{r}}, \quad (20)$$

where N is the number of unit cells and $b_{D/D',\mu,\vec{q}}^{\dagger}$ ($b_{D/D',\mu,\vec{q}}$) is the creation (annihilation) operator of a phonon with a wave vector $\vec{q}$ in the mode μ around the Dirac point D or D'. $\omega_\mu(\vec{q})$ is the corresponding frequency, which will be taken hereafter equal to the highest value of the frequency zone boundary optical modes $\hbar\omega_\mu(\vec{q})=\hbar\omega_K=161$ meV.

To highlight the role of the electronic band structure on EPC, we will assume that the phonon dispersion is not affected by the strain. We will not consider the effect of the strain on the lattice vibrations, and we will take for the K point phonon frequency the value of the unstrained graphene $\hbar\omega_K=161.2$ meV. The strain-induced change of the KA slope will then be due to the EPC via the strain-modified electronic dispersion.

Following the method described in the Appendix, we obtain the following EPC Hamiltonian:

$$H_{\rm int} = -\frac{3t}{a}\beta_K\left(1+\frac{1}{3}\epsilon\right)\begin{pmatrix}0 & \Delta_{D'}\sigma_y\\ \Delta_D\sigma_y & 0\end{pmatrix}, \quad (21)$$

where σ_y is the Pauli matrix, $\beta_K=-\frac{b}{t}\frac{\partial t}{\partial b}$, and $\Delta_{D/D'}$ is given by

$$\Delta_{D/D'} = \sqrt{\frac{\hbar}{2NM\omega_K}}\sum_{\vec{q}}\left(b_{D/D',\vec{q}} + b_{D'/D,-\vec{q}}^{\dagger}\right)e^{i\vec{q}\cdot\vec{q}}. \quad (22)$$

For $\epsilon=0$, we recover the Hamiltonian derived by Suzuura and Ando [78] for undeformed graphene.

To discuss the KA strain dependence, one needs to determine the slope $\alpha_{\vec{K}}$, which depends on the EPC matrix element $g_{D',\vec{k}'=\vec{k}+\vec{q},\pi^*;D,\vec{k},\pi}$ corresponding to the transition of an electron from the occupied band (π) of the valley D to the empty band π^* at the D valley.

3. KA slope

Given the electronic states of Eq. (13), the EPC matrix element takes the form

$$|g_{D',\vec{k}'=\vec{k}+\vec{q},\pi^*;D,\vec{k},\pi}|^2 = \frac{1}{2}\left[\frac{3t}{a}\beta_K\left(1+\frac{1}{3}\epsilon\right)\right]^2 \times\frac{\hbar}{2NM\omega_K}[1-\cos(\Phi(\vec{k})-\Phi(\vec{k}'))], \quad (23)$$

where $\tan\Phi(\vec{k}')=\frac{w_y k_y'}{w_x k_x'}$ with $\vec{k}'=\vec{k}+\vec{q}$.

Considering the electronic dispersion of Eq. (11), the KA slope $\alpha_{\vec{K}}$, given by Eq. (1), becomes

$$\alpha_{\vec{K}} = 4\left[\frac{3t}{a}\beta_K\left(1+\frac{1}{3}\epsilon\right)\right]^2\frac{\hbar}{2NM\omega_K}\frac{S'}{(2\pi)^2} \times\lim_{\vec{q}\to\vec{0}}\frac{1}{q}\int_{k<km}d^2k\left[\frac{1}{\sqrt{w_x^2k_x^2+w_y^2k_y^2}} - \frac{1+\cos(\Phi(\vec{k})+\Phi(\vec{k}'))}{\vec{w}_0\cdot\vec{q}+\sqrt{w_x^2k_x^2+w_y^2k_y^2}+\sqrt{w_x^2(k_x+q_x)^2+w_y^2(k_y+q_y)^2}}\right], \quad (24)$$

where S' is the total surface of the deformed lattice.

Introducing the components $\tilde{k}_x = w_x k_x$, $\tilde{k}_y = w_y k_y$, and the dimensionless variable $\tilde{y} = \frac{\tilde{k}}{\sqrt{w_x w_y} q}$ and setting $\Phi = \Phi(\vec{k})$ and $\Phi' = \Phi(\vec{k}')$, the integral in Eq. (24) takes the form

$$I(\varphi,\epsilon) = \frac{1}{w}\int_0^\infty d\tilde{y}\int_0^{2\pi} d\Phi \left\{ \frac{1}{\sqrt{\tilde{w}_x \tilde{w}_y}} - \tilde{y}[1+\cos(\Phi-\Phi')] \times f^{-1}(\tilde{y},\Phi)\right\}, \tag{25}$$

where $w = \frac{3}{2}at$ and the function $f(\tilde{y},\Phi)$ is given by

$$f(\tilde{y},\Phi) = \tilde{w}_{0x}\cos\varphi + \tilde{y}\sqrt{\tilde{w}_x\tilde{w}_y} + \left[\tilde{w}_x\tilde{w}_y\tilde{y}^2 + \tilde{w_x}^2\cos^2\varphi + \tilde{w}_y^2\sin^2\varphi + 2\tilde{y}\sqrt{\tilde{w}_x\tilde{w}_y}\left(\tilde{w}_x\cos\varphi\cos\Phi + \tilde{w}_y\sin\varphi\sin\Phi\right)\right]^{\frac{1}{2}}, \tag{26}$$

where $\varphi = (\vec{e}_x, \vec{q})$ is the phonon wave-vector angle, and $\tilde{w}_x$, $\tilde{w}_y$, and $\tilde{w}_{0x}$ are dimensionless parameters corresponding to the normalization, by $\frac{3}{2}at$, of respectively w_x, w_y, and w_{0x}. Φ' is given by

$$\Phi' = \arctan\frac{\tilde{y}\sqrt{\tilde{w}_x\tilde{w}_y}\sin\Phi + \tilde{w}_y\sin\varphi}{\tilde{y}\sqrt{\tilde{w}_x\tilde{w}_y}\cos\Phi + \tilde{w}_x\cos\varphi}. \tag{27}$$

Given Harrison's law [68], $\frac{a}{t}\frac{\partial t}{\partial a} = -\frac{2}{a^2}$, and expressing the surface S' of the deformed lattice as a function of the undeformed one, $S' = N \parallel \vec{a}_1 \times \vec{a}_2 \parallel \simeq S(1+\frac{2}{3}\epsilon)$, the prefactor in the expression of $\alpha_{\vec{K}}$ [Eq. (24)] becomes

$$C_K = \frac{\sqrt{3}a_0 t}{2\pi}\lambda_K\left(1+\frac{4}{3}\epsilon\right), \tag{28}$$

where $a_0 = \sqrt{3}a$ is the lattice parameter and λ_K is a dimensionless coupling parameter given by [78]

$$\lambda_K = \frac{36\sqrt{3}}{\pi}\frac{\hbar^2}{2Ma_0^2}\frac{1}{\hbar\omega_K}. \tag{29}$$

For $\hbar\omega_K = 161.2$ meV, $\lambda_K = \simeq 3.5\times10^{-3}$.

In the undeformed lattice, the integral given by Eq. (25) reduces to $\pi^2/2$, and taking $t = 2.68$ eV and $a_0 = 2.46$ Å gives $\alpha_{\vec{K}} = 253$ cm^{-1} Å [Eq. (24)], in agreement with numerical calculations [42,43].

In the following, we discuss the role of the electronic band structure on the strain dependence of the KA slope $\alpha_{\vec{K}}$.

III. RESULTS AND DISCUSSION

Figure 2 shows the normalized KA slope $\alpha_{\vec{K}}$ as a function of the strain. The normalization is taken with respect to the slope value for an unstrained lattice ($\epsilon = 0$). The calculations are done for compressive ($\epsilon < 0$) and tensile ($\epsilon > 0$) deformations along the armchair y axis. The phonon wave vector is taken along the x axis ($\varphi = 0$).

According to Fig. 2, the KA becomes more pronounced for tensile deformation. $\alpha_{\vec{K}}$ increases by about 20% (50%) for a strain of 5% (10%). However, a compressive deformation reduces the KA slope. This behavior can be understood from the electronic band structure given by Eq. (11).

Let us first disregard the tilt parameter w_{0x}. The shape of the Dirac cones depends on the electron velocities $v_x = \frac{w_x}{\hbar} \sim v_F(1+\frac{2}{3}\epsilon)$ and $v_y = \frac{w_y}{\hbar} \sim v_F(1-\frac{4}{3}\epsilon)$ [Eq. (10)], where v_F is the Fermi velocity in the unstrained lattice [68]. Therefore, the electron velocity v_y (v_x) along (perpendicular to) the strain direction decreases (increases) with the tensile deformation.

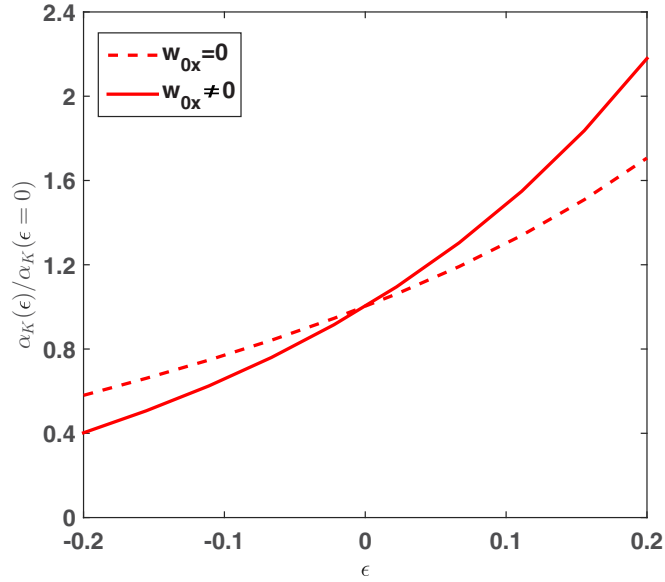

FIG. 2. KA slope $\alpha_{\vec{K}}$ as a function of strain. The data are normalized with respect to the value of $\alpha_{\vec{K}}$ for the unstrained graphene ($\epsilon = 0$). The solid line corresponds to the deformed Dirac cones including anisotropy and tilt effects while the dashed line is calculated for the untilted cones [$w_{0x} = 0$ in Eq. (11)]. The phonon wave vector is along the x axis ($\varphi = 0$).

We consider the phonon-mediated intervalley electron scattering at a constant energy E_L close to the Dirac points, as in the case of the double-resonance Raman peak 2D, for which E_L is the light excitation energy [24,28,31]. For unstrained graphene, the momentum cutoff k_m in Eq. (24) could be related to E_L as $E_L \sim \hbar v_F k_m$. Regarding the deformed Brillouin zone and the distorted Dirac cones, the intervalley processes become anisotropic.

Figure 3 shows that for a tensile strain the number of electron-hole pairs involved in the intervalley scatterings is enhanced (reduced) along the y (x) axis compared to the undeformed lattice. Actually, this anisotropic scattering is schematically equivalent to exciting an electron from the π band of the unstrained lattice with a higher (lower) energy along the k_y (k_x) axis.

The tensile renormalization of v_y is more pronounced than that of v_x, which means that globally the area of the electron wave vector $\vec{k}$ delimited by the equiexcitation energy contour E_L is larger than that in unstrained graphene, which furthers the electron-phonon scatterings and enhances the KA slope $\alpha_{\vec{K}}$, as shown in Fig. 2.

For a compressive strain, the electron-phonon interaction is reduced since the deformation affects much more the processes along the y axis, for which the number of created electron-hole pairs is reduced regarding the strain-induced enhancement of the electron velocity v_y.

Let us now discuss the role of the Dirac cone tilt. According to Fig. 2, the KA for a tensile strain is more marked in

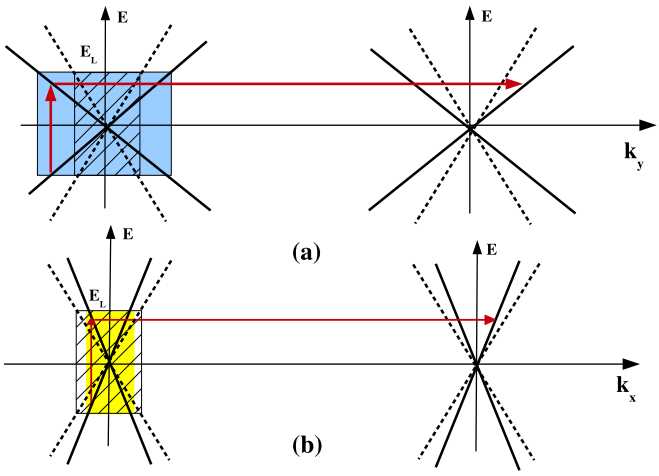

FIG. 3. Schematic representations of the intervalley phonon-mediated electronic transitions along the k_y (a) and k_x (b) axes at a given excitation energy E_L. The dashed (solid) lines represent the Dirac cones of the unstrained (strained) graphene. The Fermi velocity v_y (v_x) along (perpendicular) to the strain direction ($y'y$) is reduced (enhanced) compared to the isotropic case. This leads to more (fewer) electron-hole pairs contributing to the intervalley processes. The colored and dashed areas give the extension of the electronic states contributing to the intervalley transitions around anisotropic and isotropic Dirac cones, respectively.

the presence of the tilt while it is reduced for a compressive deformation. To explain this behavior, we plot in Fig. 4 the electronic dispersion, given by Eq. (11), along the k_x axis around the Dirac points in the direction DMD' for unstrained graphene and deformed lattices under a tensile ($\epsilon = 0.2$) and

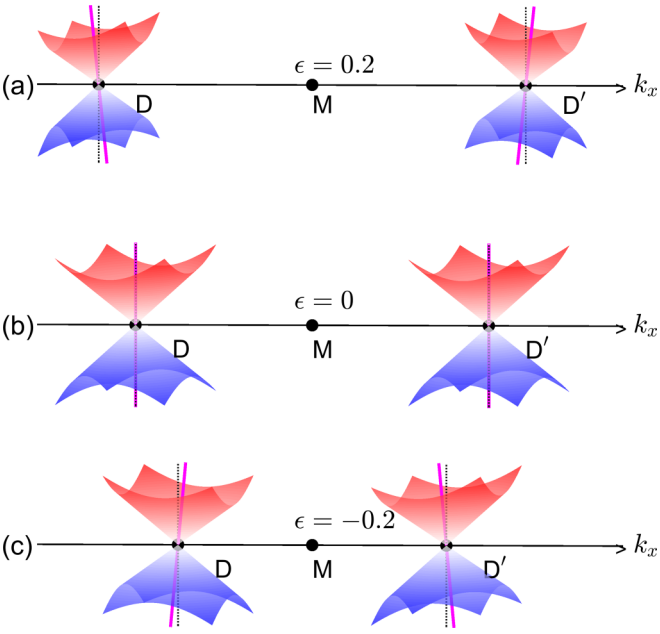

FIG. 4. Dirac cones in strained graphene [(a) and (c)] and in an undeformed lattice (b). The colored axis gives the tilt direction of the Dirac cone compared to the untilted case (dashed axis). Under a tensile (compressive) deformation, the Dirac cones, along the DMD' direction, are tilted toward the Γ (M) point.

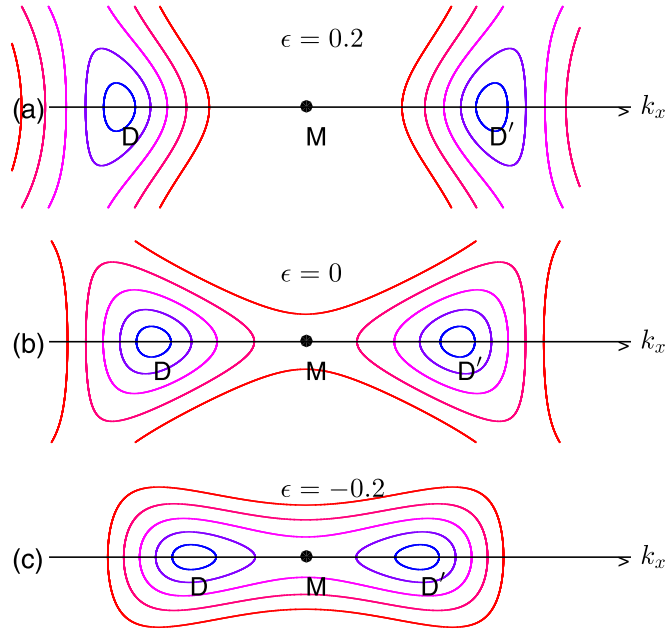

FIG. 5. Isoenergy contours along the k_x axis for strained (a),(c) and undeformed (b) graphene.

a compressive deformation ($\epsilon = -0.2$). The positions and the shape of the deformed Dirac cones are determined using the whole band structure of the quinoid lattice [68]. The Dirac cones move toward (away from) each other under a compressive (tensile) deformation [69].

The corresponding isoenergy contours are depicted in Fig. 5 showing that, along the DMD' direction, the curvature of these contours is more affected for the outer (inner) electronic states under a tensile (compressive) deformation. By outer and inner states we refer, respectively, to the states connected by a phonon wave vector $q_{\text{out}} > k_D$ and $q_{\text{in}} < k_D$. For reasons of clarity, we schematically represented in Fig. 6 the band structure depicted in Fig. 4(a).

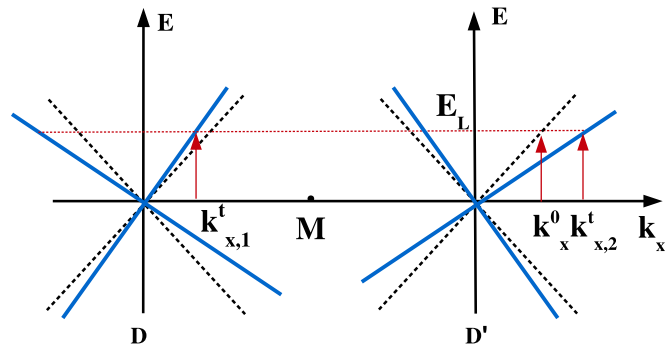

FIG. 6. Intervalley phonon-mediated electronic transitions along the k_x direction under a tensile deformation and at the excitation energy E_L indicated by the red dashed line. The dashed cones represent the nontilted case with a Fermi velocity v_x while the blue cones have also the same velocity v_x but are tilted due to the term w_{0x} in Eq. (11). k^0_x, $k^t_{x,1}$, and $k^t_{x,2}$, indicated by the arrows, are the electronic states of, respectively, the unstrained and deformed lattices corresponding to the excitation energy E_L.

For a tensile deformation, the outer states are in the tilting direction of the Dirac cones as shown in Fig. 6, where we set k_x^0 as the electron wave vector corresponding to the excitation energy E_L in the nontilted case, namely $E_L = w_x k_x^0$. We denote by $k_{x,1}^t$ and $k_{x,2}^t$ the wave vectors ascribed to the tilted cone in the D valley [$\xi = +1$ in Eq. (11)] given by

$$E_L = (w_{0x} + w_x)k_{x,1}^t, \quad E_L = (w_x - w_{0x})k_{x,2}^t, \tag{30}$$

with $w_{0x} \sim 0.6\,\epsilon\, w_x$ [Eq. (11)].

The area of the equienergy contour increases for the tilted cone since $k_{x,2}^t - k_x^0 > k_{x,1}^t - k_x^0$, which gives rise to an enhanced number of electron-hole pairs. As a consequence, the electron-phonon interaction increases, which yields the enhancement of the KA parameter $\alpha_{\vec{K}}$. It is worth noting that the electronic states along the k_y axis are not affected by the tilt of Dirac cones.

According to Fig. 6, this enhancement is due to the so-called *outer* intervalley processes involving phonons with wave vectors $q_{\text{out}} > k_D$. The dominance of the inner or outer processes in the double-resonance 2D Raman peak has been a hot topic of debate. Early experimental and numerical studies have argued that the outer phonons contribute mostly to the uniaxial strain-induced splitting of the 2D mode [36,81,82]. This outcome was contradicted by later findings based on numerical calculations and highlighting the dominance of the inner processes [19,27,30]. Narula *et al.* [31] have revoked the dominance of both types of phonons, and they showed, through a numerical study, that the dominant phonon wave vector is highly anisotropic and the distinction between inner and outer processes is irrelevant. It is worthwhile to stress that the above-mentioned numerical calculations take into account the strain-induced change of the phonon dispersion, which is not included in the present work. Our result shows that the tensile modified electronic dispersion gives rise to a dominance of the outer phonons in the electron-phonon interaction process, and this dominance is due to the tilt of Dirac cones.

On the other hand, Narula *et al.* [31] have found that the splitting of the 2D peak under a uniaxial tensile strain cannot originate only from the shift of the Dirac points. This result is in agreement with our work showing that the number of electron-hole pairs involved in the electron-phonon interaction process is independent of the Dirac cone position. This process depends basically on the shape of the equiexcitation energy contours governed by the parameters w_x and w_y and the tilt factor $\vec{w}_0$ [Eq. (11)].

The strain dependence of the KA depicted in Fig. 2 could shed light on the anisotropic mechanical properties of strained graphene. Ni *et al.* [55] have reported, based on molecular dynamics models, that the AC tensile deformation causes the fracture of graphene sooner than a tensile applied along the zigzag (ZZ) edge. This anisotropic behavior was ascribed, by the authors, to different changes of the C-C bond angles. A larger critical strain along the ZZ axis was also reported in Refs. [54,60]. In the following, we show that the KA could be responsible for the anisotropic failure mechanism of the graphene sheet.

In Fig. 7, we depicted a schematic representations of the lattice deformed under AC and ZZ tensile, where t denotes the hopping integral between first neighbors in an unstrained system, and t' (t'_{ZZ}) is the hopping integral under an AC (ZZ) tensile.

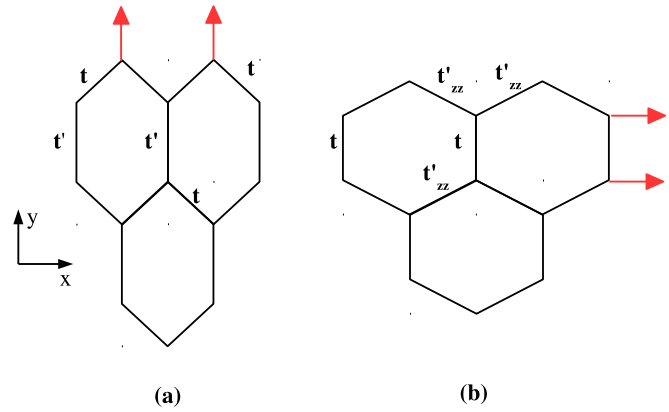

FIG. 7. Deformed honeycomb lattice under a tensile applied along the armchair direction (a) and the zigzag one (b). The arrows indicate the direction of the tensile deformation. t, t', and t'_{ZZ} are the hopping integrals between first neighboring atoms.

The lattice deformed under a ZZ tensile could be regarded as that obtained under a compressive AC strain with unstrained hopping $\tilde{t} = t'_{ZZ}$ and a strain-modified hopping integral $\tilde{t}' = t$ with $\tilde{t}' = \tilde{t}(1 + 2|\epsilon|)$ [Eq. (8)]. The corresponding KA slope is that given by Eq. (24) by changing t by $\tilde{t}$ and t' by $\tilde{t}'$.

As shown in Fig. 2, the KA is reduced, under a compressive strain, compared to the undeformed case ($\epsilon = 0$). Moreover, changing t by $\tilde{t} = t'_{ZZ} < t$ in Eq. (24) reduces the prefactor term and then weakens the KA. As a consequence, the KA is reduced for a ZZ tensile strain compared to the AC one. This result is consistent with the anisotropic frequency shifts of the TO phonon mode under strain along ZZ and AC directions obtained within first-principles calculations in Ref. [49]. We then propose that the KA should be taken into consideration to explain the relatively large critical strain along the ZZ edges, which is due to the hardening of the TO phonon modes at the K point induced by the weakening of the KA.

Regarding the unique mechanical properties of graphene, extensive studies have been carried out to understand, in particular, the anisotropic mechanical failure of the graphene sheet along the ZZ and AC directions [20,50,54,59,60,65]. Several atomistic studies based on molecular dynamics calculations have revealed that graphene exhibits greater toughness and strength along the ZZ direction compared to the AC one. The origin of this direction-dependent behavior was ascribed to anisotropic bond stretching and bond bending deformations [20,54,65]. Under strain, the CC bonds along the ZZ and AC directions are different. This chirality dependence is more marked at low temperature [58].

DFT calculations [59] showed that during the failure process, the crack direction is anisotropic. The zigzag crack occurs along a straight line while the AC crack is irregular regarding the geometry of the CC bonds.

Recently, the evolution of the CC bond lengths and the bond angles of graphene, under uniaxial strain, has been studied by DFT calculations in view of understanding the anisotropic value of the Poisson ratio [66]. The results showed

that these geometric key parameters behave differently under strain applied along the ZZ and the AC directions. This chirality was ascribed to the strain dependence of the electron localization functions.

The outcomes of these studies bring out the relevance of the geometrical parameter in the anisotropic behavior of the mechanical failure of graphene. According to Fig. 7, the CC bond lengths and angles are different for strain aligned along the AC and the ZZ edges, which is in agreement with numerical studies. However, our model is not limited to the geometrical framework. We argued that, for a deformation along the ZZ direction, the KA is smeared out, which enhances the TO phonon frequency at the K point and strengthens the collective lattice vibrations, which results in a larger critical loading along the ZZ edge compared to that along the AC direction. A quantitative comparison of our results with those obtained by DFT calculations is not relevant since we did not include the Poisson ratio and the shear strain component. Moreover, our calculations did not take into consideration the strain-modified phonon dispersion.

It is worth noting that the lattice softening resulting from the enhancement of the KA under tensile uniaxial strain could be counterbalanced by charge doping as reported by Si *et al.* [48]. They found a peculiar behavior of the doping-induced frequency shifts of the TO modes at the K point. In strained graphene, this shift is remarkably greater than that in an unstrained lattice. The authors mentioned that the origin of this large difference is not clear within the framework of their first-principles calculations. In the next, we give, based on schematic representations of the doped graphene band structure, a possible interpretation of this feature.

Figure 8(a) shows the electron-hole pairs involved in the intervalley phonon-mediated processes in unstrained graphene for a given excitation energy E_L and at charge neutrality. By electron doping at $E_F < E_L$ [Fig. 8(b)], the number of electron-hole pairs contributing to the intervalley processes is reduced due to the Pauli principle, which explains the hardening of the phonon frequency by doping unstrained graphene [48].

Under a uniaxial tensile, the Fermi energy is renormalized as [68]

$$E_F^* = E_F\left(1 - \frac{1}{3}\epsilon\right). \tag{31}$$

In Fig. 8, we represented the electronic states involved in the intervalley processes along the k_y direction, which give, as discussed above, a dominant contribution to the KA under tensile deformation. The number of electronic states blocked by the Pauli principle in the strained lattice is greater than that for the undeformed case. Indeed, these states are in the interval $\Delta k_y = E_F^*/w_y \sim (1+\epsilon)E_F/w$, while in the unstrained lattice the locked states are within the interval $\Delta k_y^0 = E_F/w$, where $w = \frac{3}{2}at$ [Eq. (11)].

For $\epsilon > 0$, $\Delta k_y > \Delta k_y^0$. This leads to a larger number of blocked intervalley processes in graphene under uniaxial tensile strain, which is consistent with the result of Ref. [48]. Moreover, the KA is expected to be weakened by doping regarding the enhancement of Δk_y with E_F, which is in agreement with Refs. [34,48].

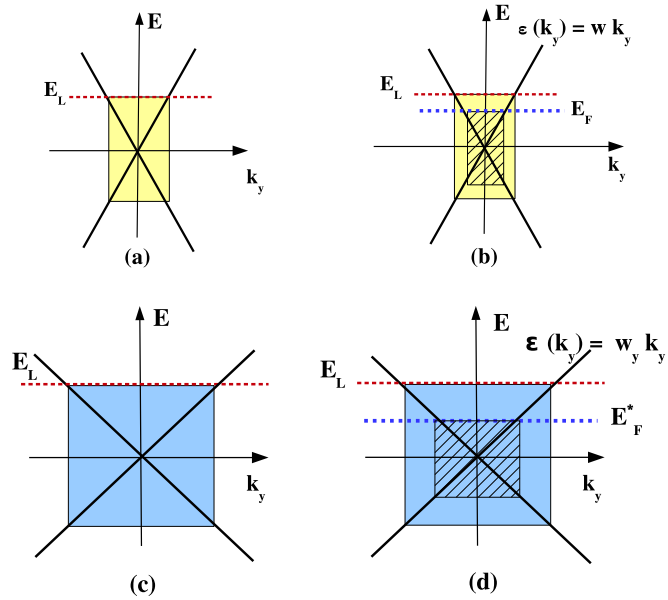

FIG. 8. Schematic representation of the electronic states along the k_y direction involved in the intervalley phonon-mediated processes for a given excitation energy E_L. The undoped system corresponds to the cases (a) and (c) where the Fermi level is at the Dirac point while the doped system is shown in (b) and (d). The upper figures [(a) and (b)] correspond to the unstrained lattice while the lower ones [(c) and (d)] describe a lattice under a tensile deformation. w denotes the slope of the isotropic Dirac cone, while $w_y < w$ is the slope of the Dirac cone under tensile along the k_y axis. E_F^* is the strain-renormalized Fermi energy. The dashed areas correspond to the electronic states blocked by the Pauli principle.

In Fig. 9, we represent the phonon angle dependence of the normalized KA parameter for different strain values. For the unstrained lattice, the KA is isotropic with respect to the phonon wave-vector direction since the isoenergy contours are almost circular at low energy. As the strain amplitude increases, the KA becomes anisotropic with a dominant component for phonons with wave vector $\vec{q}$ along the x axis, which is perpendicular to the strain direction.

This result is in agreement with the light polarization angle dependence of the 2D Raman band reported in the literature. Several experimental and numerical studies [19,24,28] have found that the 2D peak splits under strain into two lines. Under AC strain, the intensity of the line associated with a parallel light polarization with respect to the strain direction is greater than that of the peak ascribed to the perpendicular polarization, i.e., $I_{2D}(\theta = 90°) < I_{2D}(\theta = 0°)$, where θ is the angle of the light polarization with the respect to the strain direction [28]. Since the Raman intensity depends on $|\vec{q} \times \vec{E}|$, where $\vec{q}$ is the phonon wave vector and $\vec{E}$ is the light polarization [18], the 2D band is then expected to show a large intensity for $\vec{q}$ along the direction perpendicular to the strain axis. This behavior is in agreement with our result depicted in Fig. 9 showing that the KA is enhanced for $\varphi = 0$.

Moreover, Fig. 9 shows that the KA should exhibit a minimum around the y direction ($\varphi = \pi/2$). This behavior is due to the tilt of Dirac cones, which, as discussed above, enhances the KA for electronic states along the k_x axis. According to

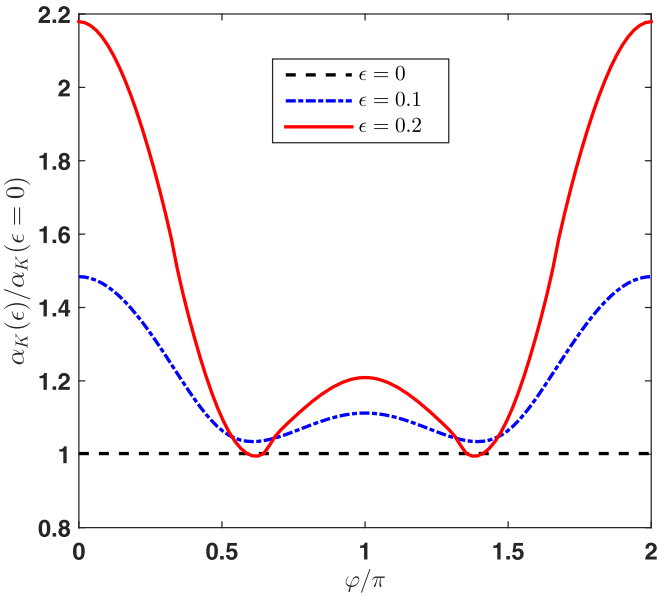

FIG. 9. Phonon angle dependence of the KA slope $\alpha_{\vec{K}}$ for different strain amplitudes. φ is the angle between the phonon wave vector $\vec{q}$ and the x axis perpendicular to the strain direction. The data are normalized with respect to the value of $\alpha_{\vec{K}}$ for $\varphi = 0$ in the unstrained lattice ($\epsilon = 0$).

Fig. 9, the KA is expected to have a relative maximum for phonons with $\varphi = \pi$, which correspond to the inner intervalley processes. As we have already shown, the latter have a minor contribution to the KA compared to the outer processes.

Figure 10 shows the KA slope as a function of the phonon angle for a tensile strain of $\epsilon = 0.2$. The solid (dashed) curve

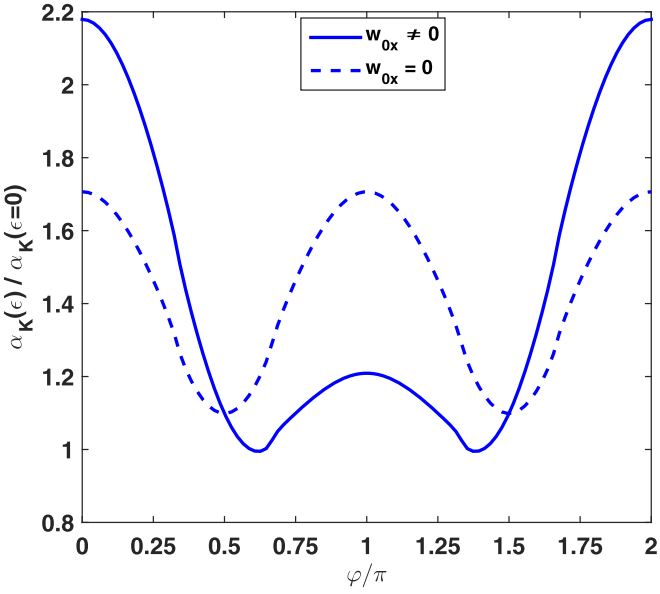

FIG. 10. Phonon angle dependence of the KA slope $\alpha_{\vec{K}}$ in the case of tilted (solid line) and nontilted (dashed line) cones. The data are normalized with respect to the value of $\alpha_{\vec{K}}$ for $\varphi = 0$ in the unstrained lattice. The calculations are done for a tensile strain $\epsilon = 0.2$.

corresponds to the case of tilted (nontilted) Dirac cones. According to this figure, the anisotropic behavior of $\alpha_{\vec{K}}$ is due to the anisotropic Fermi velocities of $v_x = w_x/\hbar$ and $v_y = w_y/\hbar$. However, the tilt parameter is responsible for the dominance of the outer intervalley phonon processes, corresponding to $\varphi = 0$, for which $\alpha_{\vec{K}}$ reaches its maximum value. The inner processes have a lower contribution associated with $\varphi = \pi$.

As mentioned by Narula *et al.*, the notion of inner and outer processes is rather confusing since they can be mapped into each other by the addition of a reciprocal-lattice vector. The authors showed, based on numerical calculations, that the dominant phonon-mediated intervalley electronic transitions are neither inner nor outer but with a significant contribution of the inner processes. To avoid any confusing nomenclature, we conclude that the intervalley processes, connecting the most deformed parts of the electronic isoenergy contours, have the dominant contribution to the KA around the Dirac points.

IV. CONCLUSION

In summary, we have presented an analytical study of the effect of the electronic dispersion relation on the KA of strained graphene. We found that, besides the shifts of the KA phonon wave vector, the strain dependence of the slope parameter $\alpha_{\vec{K}}$ describing this anomaly is substantially dependent on the electronic band structure. In particular, the KA is found to be enhanced under tensile strain by the tilt of Dirac cones. The latter furthers the so-called *outer* intervalley phonon processes. We have also found that the strain dependence of the electronic band structure is at the origin of the strong doping-induced reduction of the KA in graphene under a tensile deformation compared to the undeformed lattice. Moreover, our results show that the KA is anisotropic with respect to the phonon wave vector, which may provide insights not only on the light polarization dependence of a Raman 2D band but also on the anisotropic mechanical failure of graphene under strain.

ACKNOWLEDGMENTS

We thank M. E. Cifuentes-Quintal for stimulating discussions. We are indebted to M. E. Cifuentes-Quintal, J.-N. Fuchs, and Reza Asgari for a critical reading of the manuscript. S.H. acknowledges the kind hospitality of ICTP (Trieste, Italy) where part of the work was carried out. S.H. was supported by the Simons-ICTP associate fellowship.

APPENDIX A: EPC HAMILTONIAN BY $\vec{k} \cdot \vec{p}$ METHOD

The $\vec{k} \cdot \vec{p}$ method was used by Suzuura and Ando [78] to obtain the effective Hamiltonian describing the interaction between electrons and the zone boundary optical phonons corresponding to the highest-frequency mode, the so-called Kekulé mode. This method was also used to determine the electron-phonon interaction Hamiltonian in the case of the optical zone center phonon modes of graphene in the absence of deformation [79] and under a uniaxial strain [32].

Based on Ref. [78], we derive the EPC matrix element $g_{D',\vec{k}'=\vec{k}+\vec{q},\pi^*;D,\vec{k},\pi}$ corresponding to the transition of an electron from the occupied band (π) of the valley D to the empty band π^* at the D' valley in graphene, under uniaxial strain applied along the armchair direction.

We start with the electronic eigenproblem given by Eq. (17), where the functions $\psi_A(\vec{R}_A)$ and $\psi_B(\vec{R}_B)$ can be written in terms of the envelope functions $F_A^{D/D'}(\vec{R}_A)$ and $F_B^{D/D'}(\vec{R}_B)$ as

$$\begin{aligned}\psi_A(\vec{R}_A) &= a^\dagger(\vec{R}_A)\Phi_A(\vec{R}_A),\\ \psi_B(\vec{R}_B) &= b^\dagger(\vec{R}_B)\Phi_B(\vec{R}_B),\end{aligned} \tag{A1}$$

with

$$\begin{aligned}a(\vec{R}_A) &= \begin{pmatrix} e^{-i\vec{k}^D\cdot\vec{R}_A}\\ e^{-i\vec{k}^{D'}\cdot\vec{R}_A}\end{pmatrix}, \quad b(\vec{R}_B) = \begin{pmatrix} e^{-i\vec{k}^D\cdot\vec{R}_B}\\ -e^{-i\vec{k}^{D'}\cdot\vec{R}_B}\end{pmatrix},\\ \Phi_A(\vec{R}_A) &= \begin{pmatrix} F_A^D(\vec{R}_A)\\ F_A^{D'}(\vec{R}_A)\end{pmatrix}, \quad \Phi_B(\vec{R}_B) = \begin{pmatrix} F_B^D(\vec{R}_B)\\ F_B^{D'}(\vec{R}_B)\end{pmatrix}.\end{aligned} \tag{A2}$$

As in Ref. [78], we introduce the smoothing function $g(\vec{r})$ satisfying the following relations:

$$\begin{aligned}\sum_{\vec{R}_A} g(\vec{r}-\vec{R}_A) &= \sum_{\vec{R}_B} g(\vec{r}-\vec{R}_B) = 1,\\ f(\vec{r})g(\vec{r}-\vec{R}_A) &\simeq f(\vec{R})g(\vec{r}-\vec{R}),\end{aligned} \tag{A3}$$

where $f(\vec{r})$ is an envelope function [79]. The left-hand side of Eq. (17) can then be written, at the $\vec{R}_A$ site, as

$$\begin{aligned}&\varepsilon\, a(\vec{R}_A)a^\dagger(\vec{R}_A)F_A(\vec{r})\\ &= \varepsilon\sum_{\vec{R}_A} g(\vec{r}-\vec{R}_A)a(\vec{R}_A)a^\dagger(\vec{R}_A)F_A(\vec{r})\\ &= -\sum_{l=1}^{3} t^{(l)}\sum_{\vec{R}_A} g(\vec{r}-\vec{R}_A)a(\vec{R}_A)b^\dagger(\vec{R}_B)F_B(\vec{r}-\vec{\tau}_l)\\ &\quad -\sum_{l=1}^{6} t_{nnn}^{(l)}\sum_{\vec{R}_A} g(\vec{r}-\vec{R}_A)a(\vec{R}_A)a^\dagger(\vec{R}_A-\vec{a}_l)F_A(\vec{r}-\vec{a}_l).\end{aligned} \tag{A4}$$

For small strain amplitude, the following relations are satisfied:

$$\begin{aligned}\sum_{\vec{R}_A} g(\vec{r}-\vec{R}_A)e^{i(\vec{k}^{D'}-\vec{k}^D)\cdot\vec{R}_A} &= \sum_{\vec{R}_B} g(\vec{r}-\vec{R}_B)e^{i(\vec{k}^{D'}-\vec{k}^D)\cdot\vec{R}_B} \simeq 0,\\ \sum_{\vec{R}_A} g(\vec{r}-\vec{R}_A)e^{i\vec{k}^D\cdot\vec{R}_A} &\simeq 0.\end{aligned} \tag{A5}$$

Taking into account the lattice vibrations on the hopping integral to the first neighbor atoms, an extra term appears in the eigenproblem given by Eq. (17). This term is of the form

$$\begin{aligned}H_{\rm int}F_B(\vec{r}) = \sum_l\sum_{\vec{R}_A} g(\vec{r}-\vec{R}_A)a(\vec{R}_A)b(\vec{R}_A-\vec{\tau}_l)\left(-\frac{\partial t^{(l)}}{\partial d_l}\right)\\ \times\left(\frac{\vec{\tau}_l}{d_l}\right)\cdot(\vec{u}_A(\vec{R}_A)-\vec{u}_B(\vec{R}_A-\vec{\tau}_l))F_B(\vec{r}),\end{aligned} \tag{A6}$$

where $F_B(\vec{r}) = \begin{pmatrix} F_B^D(\vec{r})\\ F_B^{D'}(\vec{r})\end{pmatrix}$.

We consider the phonon modes around the Dirac points D and D' with wave vector $\vec{k}^{D/D'}+\vec{q}$, where $\|\vec{q}\| \ll \frac{2\pi}{a}$. We can then use the continuum limit and put in Eq. (19): $\vec{u}_A^{D/D'}(\vec{R}_A) \simeq \vec{u}_A^{D/D'}(\vec{r})$ and $\vec{u}_B^{D/D'}(\vec{R}_A-\vec{\tau}_l) \simeq \vec{u}_B^{D/D'}(\vec{r})$. Equation (A6) can then be written as

$$H_{\rm int}F_B^D(\vec{r}) = h'^{AB}_{\rm int}F_B^{D'}(\vec{r}), \tag{A7}$$

where $h'^{AB}_{\rm int}$ is given by

$$\begin{aligned}h'^{AB}_{\rm int} = \sum_l\left(-\frac{\partial t^{(l)}}{\partial d_l}\right)\left(\frac{\vec{\tau}_l}{d_l}\right)\cdot\\ \times\left[e^{-i\vec{k}^{D'}\cdot\vec{\tau}_l}\vec{u}_A^{D'}(\vec{r}) - e^{-2i\vec{k}^{D'}\cdot\vec{\tau}_l}\vec{u}_B^{D'}(\vec{r})\right],\end{aligned} \tag{A8}$$

with $t^{(1)}=t^{(2)}=t$, $t^{(3)}=t'=t(1-2\epsilon)$, $\vec{k}^{D'}\cdot\vec{\tau}_3=0$, and $\vec{k}^{D'}\cdot\vec{\tau}_1 = -\vec{k}^{D'}\cdot\vec{\tau}_2 = -\theta$, where $\theta = \arccos(-\frac{t'}{2t}) = a\frac{\sqrt{3}}{2}k_x^D$.

$h'^{AB}_{\rm int}$ then takes the following form:

$$\begin{aligned}h'^{AB}_{\rm int} = -i\frac{3}{2}\frac{\partial t}{\partial a}\Bigg[\left(1+\frac{2}{3}\epsilon\right)u_{Ax}^{D'}(\vec{r}) + iu_{Ay}^{D'}(\vec{r})\\ +\left(1-\frac{4}{3}\epsilon\right)u_{Bx}^{D'}(\vec{r}) - i(1+2\epsilon)u_{By}^{D'}(\vec{r})\Bigg],\end{aligned} \tag{A9}$$

where we considered the limit of small strain amplitude ($|\epsilon| \ll 1$).

To bring out the signature of the electronic dispersion on the EPC, we assume that the phonon dispersion at the K' point is not affected by the strain. This means that the phonon polarization of the highest frequency optical mode is [78] $\vec{e}_{D'} = \vec{e}_{K'} = \frac{1}{2}\begin{pmatrix}1\\-i\\1\\i\end{pmatrix}$.

The matrix element $h'^{AB}_{\rm int}$ becomes

$$h'^{AB}_{\rm int} = -3i\frac{\partial t}{\partial a}\left(1+\frac{1}{3}\epsilon\right)\vec{e}^{\,0}_{D'}\cdot\vec{U}_{D'}, \tag{A10}$$

where

$$\vec{U}_{D'} = \begin{pmatrix}\vec{u}_A^{D'}\\ \vec{u}_B^{D'}\end{pmatrix} = \sqrt{\frac{\hbar}{2NM\omega_K}}\vec{e}_{K'}\sum_{\vec{q}}(b_{D,\vec{q}}+b^\dagger_{D,-\vec{q}})e^{i\vec{q}\cdot\vec{r}} \tag{A11}$$

and $\vec{e}^{\,0}_{D'} = \frac{1}{2(1+\frac{1}{3}\epsilon)}\begin{pmatrix}1+\frac{2}{3}\epsilon\\ -i\\ 1-\frac{4}{3}\epsilon\\ i(1+2\epsilon)\end{pmatrix}$.

The effective interaction Hamiltonian takes a form similar to that found by Suzzura and Ando [78]:

$$H_{\rm int} = -3\frac{t}{a}\beta_K\left(1+\frac{1}{3}\epsilon\right)\begin{pmatrix}0 & \Delta_{D'}\sigma_y\\ \Delta_D\sigma_y & 0\end{pmatrix}, \tag{A12}$$

with $\Delta_{D'} = \vec{e}^{\,0}_{D'}\cdot\vec{U}_{D'}$, $\beta_K = -\frac{a}{t}\frac{\partial t}{\partial a}$, and σ_y is the Pauli matrix.

[1] A. H. Castro Neto, F. Guinea, N. M. R. Peres, K. S. Novoselov, and A. K. Geim, Rev. Mod. Phys. **81**, 109 (2009).

[2] M. S. Nevius, M. Conrad, F. Wang, A. Celis, M. N. Nair, A. Taleb-Ibrahimi, A. Tejeda, and E. H. Conrad, Phys. Rev. Lett. **115**, 136802 (2015).

[3] V. N. Kotov, B. Uchoa, V. M. Pereira, F. Guinea, and A. H. Castro Neto, Rev. Mod. Phys. **84**, 1067 (2012).

[4] G. Naumis, S. Barraza-Lopez, M. Oliva-Leyva, and H. Terrones, Rep. Prog. Phys. **80**, 096501 (2017).

[5] C. Si, Z. Suna, and F. Liu, Nanoscale **8**, 3207 (2016).

[6] R. Roldán, A. Castellanos-Gomez, E. Cappelluti, and F. Guinea, J. Phys.: Condens. Matter **27**, 313201 (2015).

[7] M. A. Bisset, M. Tsuji, and H. Ago, Phys. Chem. Chem. Phys. **16**, 11124 (2014).

[8] F. Guinea, Solid State Commun. **152**, 1437 (2012).

[9] V. M. Pereira and A. H. Castro Neto, Phys. Rev. Lett. **103**, 046801 (2009).

[10] N. Levy, S. A. Burke, K. L. Meaker, M. Panlasigui, A. Zettl, F. Guinea, A. H. Castro Neto, and M. F. Crommie, Science **329**, 544 (2010).

[11] C. Si, Z. Liu, W. Duan, and F. Liu, Phys. Rev. Lett. **111**, 196802 (2013).

[12] B. Uchoa and Y. Barlas, Phys. Rev. Lett. **111**, 046604 (2013).

[13] C. Lee, X. Wei, J. W. Kysar, and J. Hone, Science **321**, 385 (2008).

[14] V. M. Pereira, A. H. Castro Neto, and N. M. R. Peres, Phys. Rev. B **80**, 045401 (2009).

[15] N. Z. Hua, Y. Ting, L. Y. Hao, W. Y. Ying, F. Y. Ping, and S. Z. Xiang, ACS Nano **3**, 483 (2009).

[16] F. Guinea, M. I. Katsnelson, and A. K. Geim, Nat. Phys. **6**, 30 (2010).

[17] C-L. Li, AIP Adv. **4**, 087119 (2014).

[18] A. C. Ferrari and D. M. Basko, Nat. Nanotechnol. **8**, 235 (2013).

[19] M. Huang, H. Yan, T. F. Heinz, and J. Hone, Nano Lett. **10**, 4074 (2010).

[20] Z. H. Ni, W. Chen, X. F. Fan, J. L. Kuo, T. Yu, A. T. S. Wee, and Z. X. Shen, Phys. Rev. B **77**, 115416 (2008).

[21] Z. H. Ni, T. Yu, Y. H. Lu, Y. Y. Wang, Y. P. Feng, and Z. X. Shen, ACS Nano **2**, 2301 (2008).

[22] T. M. G. Mohiuddin, A. Lombardo, R. R. Nair, A. Bonetti, G. Savini, R. Jalil, N. Bonini, D. M. Basko, C. Galiotis, N. Marzari, K. S. Novoselov, A. K. Geim, and A. C. Ferrari, Phys. Rev. B **79**, 205433 (2009).

[23] O. Frank, G. Tsoukleri, J. Parthenios, K. Papagelis, I. Riaz, R. Jalil, K. S. Novoselov, and C. Galiotis, ACS Nano **4**, 3131 (2010); O. Frank, G. Tsoukleri, I. Riaz, K. Papagelis, J. Parthenios, A. C. Ferrari, A. K. Geim, K. S. Novoselov, and C. Galiotis, Nat. Commun. **2**, 255 (2011).

[24] O. Frank, M. Mohr, J. Maultzsch, C. Thomsen, I. Riaz, R. Jalil, K. S. Novoselov, G. Tsoukleri, J. Parthenios, K. Papagelis, L. Kavan, and C. Galiotis, ACS Nano **5**, 2231 (2011).

[25] J.-U. Lee, D. Yoon, and H. Cheong, Nano Lett. **12**, 4444 (2012).

[26] C. W. Huang, R. J. Shiue, H. C. Chui, W. H. Wang, J. K. Wang, Y. Tzeng, and C. Y. Liu, Nanoscale **5**, 9626 (2013).

[27] D. Yoon, Y. W. Son, and H. Cheong, Phys. Rev. Lett. **106**, 155502 (2011).

[28] V. N. Popov and P. Lambin, Carbon **54**, 86 (2013); Phys. Rev. B **87**, 155425 (2013).

[29] C. Thomsen, S. Reich, and P. Ordejón, Phys. Rev. B **65**, 073403 (2002).

[30] M. Mohr, J. Maultzsch, and C. Thomsen, Phys. Rev. B **82**, 201409(R) (2010).

[31] R. Narula, N. Bonini, N. Marzari, and S. Reich, Phys. Rev. B **85**, 115451 (2012).

[32] M. Assili and S. Haddad, Phys. Rev. B **90**, 125401 (2014).

[33] C. Neumann, S. Reichardt, P. Venezuela, M. Drögeler, L. Banszerus, M. Schmitz, K. Watanabe, T. Taniguchi, F. Mauri, B. Beschoten, S. V. Rotkin, and C. Stampfer, Nat. Commun. **6**, 8429 (2015).

[34] X. Wang, J. W. Christopher, and A. Swan, Sci. Rep. **7**, 13539 (2017).

[35] S. Reich and C. Thomsen, Philos. Trans. R. Soc. London, Ser. A **362**, 2271 (2004).

[36] C. Thomsen and S. Reich, Phys. Rev. Lett. **85**, 5214 (2000).

[37] D. M. Basko, Phys. Rev. B **78**, 125418 (2008).

[38] R. Saito, A. Jorio, A. G. Souza Filho, G. Dresselhaus, M. S. Dresselhaus, and M. A. Pimenta, Phys. Rev. Lett. **88**, 027401 (2001).

[39] J. Maultzsch, S. Reich, and C. Thomsen, Phys. Rev. B **70**, 155403 (2004).

[40] P. Venezuela, M. Lazzeri, and F. Mauri, Phys. Rev. B **84**, 035433 (2011).

[41] W. Kohn, Phys. Rev. Lett. **2**, 393 (1959).

[42] S. Piscanec, M. Lazzeri, F. Mauri, A. C. Ferrari, and J. Robertson, Phys. Rev. Lett. **93**, 185503 (2004).

[43] M. Lazzeri and F. Mauri, Phys. Rev. Lett. **97**, 266407 (2006).

[44] M. Lazzeri, C. Attaccalite, L. Wirtz, and F. Mauri, Phys. Rev. B **78**, 081406(R) (2008).

[45] K.-i. Sasaki, M. Yamamoto, S. Murakami, R. Saito, M. S. Dresselhaus, K. Takai, T. Mori, T. Enoki, and K. Wakabayashi, Phys. Rev. B **80**, 155450 (2009).

[46] S. K. Saha, U. V. Waghmare, H. R. Krishnamurthy and A. K. Sood, Phys. Rev. B **76**, 201404(R) (2007); F. Forster, A. Molina-Sanchez, S. Engels, A. Epping, K. Watanabe, T. Taniguchi, L. Wirtz, and C. Stampfer, *ibid.* **88**, 085419 (2013); F. de Juan and H. A. Fertig, *ibid.* **85**, 085441 (2012).

[47] C. A. Marianetti and H. G. Yevick, Phys. Rev. Lett. **105**, 245502 (2010).

[48] C. Si, W. Duan, Z. Liu, and F. Liu, Phys. Rev. Lett. **109**, 226802 (2012).

[49] M. E. Cifuentes-Quintal, O. de la Peña-Seaman, R. Heid, R. de Coss, and K.-P. Bohnen, Phys. Rev. B **94**, 085401 (2016).

[50] F. Liu, P. Ming, and J. Li, Phys. Rev. B **76**, 064120 (2007).

[51] X. Wei, B. Fragneaud, C. A. Marianetti, and J. W. Kysar, Phys. Rev. B **80**, 205407 (2009).

[52] H. Zhao, K. Min, and N. R. Aluru, Nano Lett. **9**, 3012 (2009).

[53] C. K. Gan and D. J. Srolovitz, Phys. Rev. B **81**, 125445 (2010).

[54] Y. Gao and P. Hao, Physica E **41**, 1561 (2009).

[55] Z. Ni, H. Bu, M. Zou, H. Yi, K. Bi, and Y. Chen, Physica B **405**, 1301 (2010).

[56] Y. Li, X. Jiang, Z. Liu, and Z. Liu, Nano Res. **3**, 545 (2010).

[57] N. Rosenkranz, M. Mohr, and C. Thomsen, Ann. Phys. (Berlin) **523**, 137 (2011).

[58] K. Min and N. R. Aluru, Appl. Phys. Lett. **98**, 013113 (2011).

[59] M. Xu, A. Tabarraei, J. T. Paci, J. Oswald, and T. Belytschko, Int. J. Fract. **173**, 163 (2012).

[60] G. Cao, Polymers **6**, 2404 (2014).

[61] Y. I. Jhon, Y. M. Jhon, G. Y. Yeom, and M. S. Jhon, Carbon **66**, 619 (2014).

[62] A. V. Orlov and I. A. Ovidko, Rev. Adv. Mater. Sci. **40**, 249 (2015).
[63] K. Kim, V. I. Artyukhov, W. Regan, Y. Liu, M. F. Crommie, B. I. Yakobson, and A. Zettl, Nano Lett. **12**, 293 (2012).
[64] Y. Zhao, S. Dong, P. Yu, and J. Zhao, Acta Mech. Sin. **34**, 542 (2018).
[65] M. Z. Hossain, T. Ahmed, B. Silverman, M. S. Khawaja, J. Calderon, A. Rutten, and S. Tse, J. Mech. Phys. Solids **110**, 118 (2018).
[66] Z. Qin, G. Qin, and M. Hu, Nanoscale **10**, 10365 (2018).
[67] S. Li, Y. Wang, H. Wang, and Y. Chen, Carbon **126**, 404 (2018).
[68] M. O. Goerbig, J.-N. Fuchs, G. Montambaux, and F. Piéchon, Phys. Rev. B **78**, 045415 (2008).
[69] M. Goerbig, Rev. Mod. Phys. **83**, 1193 (2011).
[70] M. E. Cifuentes-Quintal (private communication).
[71] Y. Betancur-Ocampo, M. E. Cifuentes-Quintal, G. Cordourier-Maruri, and R. de Coss, Ann. Phys. (N.Y.) **359**, 243 (2015).
[72] A. Kobayashi, S. Katayama, Y. Suzumura, and H. Fukuyama, J. Phys. Soc. Jpn. **76**, 034711 (2007).
[73] F. M. D. Pellegrino, G. G. N. Angilella, and R. Pucci, Phys. Rev. B **84**, 195407 (2011).
[74] J. P. F. LeBlanc and J. P. Carbotte, Phys. Rev. B **87**, 205407 (2013).
[75] V. M. Pereira, A. H. Castro Neto, H. Y. Liang, and L. Mahadevan, Phys. Rev. Lett. **105**, 156603 (2010).
[76] M. A. H. Vozmediano, M. I. Katsnelson, and F. Guinea, Phys. Rep. **496**, 109 (2010).
[77] M. Oliva-Leyva and G. G. Naumis, Phys. Rev. B **88**, 085430 (2013).
[78] H. Suzuura and T. Ando, J. Phys. Soc. Jpn. **77**, 044703 (2008).
[79] T. Ando, J. Phys. Soc. Jpn. **75**, 084713 (2006).
[80] P. Marconcini and M. Macucci, La Rivista del Nuovo Cimento **34**, 489 (2011).
[81] A. C. Ferrari, J. C. Meyer, V. Scardaci, C. Casiraghi, M. Lazzeri, F. Mauri, S. Piscanec, D. Jiang, K. S. Novoselov, S. Roth, and A. K. Geim, Phys. Rev. Lett. **97**, 187401 (2006).
[82] J. Kurti, V. Zolyomi, A. Gruneis, and H. Kuzmany, Phys. Rev. B **65**, 165433 (2002).